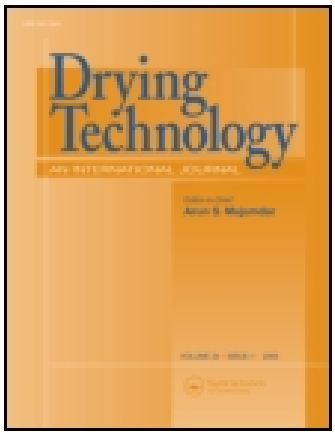

Drying Technology: An International Journal
Publication details, including instructions for authors and subscription information:
http://www.tandfonline.com/loi/ldrt20

Modeling the Drying of Grass Seeds (Brachiaria brizantha) in Fluidized Beds

A. C. Rizzi Jr. [a] , E. F. Costa Jr. [b] , J. T. Freire [a] & M. L. Passos [a]
[a] Programa de Pós-Graduação em Engenharia Química, Centro de Secagem de Pastas, Suspensões e Sementes , Universidade Federal de São Carlos , São Carlos, SP, Brazil
[b] Mestrado em Engenharia Industrial, UNILESTMG , Coronel Fabriciano, MG, Brazil
Published online: 10 Apr 2007.

To cite this article: A. C. Rizzi Jr. , E. F. Costa Jr. , J. T. Freire & M. L. Passos (2007) Modeling the Drying of Grass Seeds (Brachiaria brizantha) in Fluidized Beds, Drying Technology: An International Journal, 25:1, 123-134, DOI: 10.1080/07373930601160957

To link to this article: http://dx.doi.org/10.1080/07373930601160957

Drying Technology, 25: 123–134, 2007

ISSN: 0737-3937 print/1532-2300 online
DOI: 10.1080/07373930601160957

Taylor & Francis
Taylor & Francis Group

Modeling the Drying of Grass Seeds (*Brachiaria brizantha*) in Fluidized Beds

A. C. Rizzi Jr.,[1] E. F. Costa Jr.,[2] J. T. Freire,[1] and M. L. Passos[1]

[1]*Programa de Pós-Graduação em Engenharia Química, Centro de Secagem de Pastas, Suspensões e Sementes, Universidade Federal de São Carlos, São Carlos, SP, Brazil*
[2]*Mestrado em Engenharia Industrial, UNILESTMG, Coronel Fabriciano, MG, Brazil*

A modified three-phase model is developed to simulate the drying of *Brachiaria brizantha* in fluidized beds. In this new model, the constitutive equation of drying kinetics is formulated including both the constant rate and the falling rate mechanisms; the seed shrinkage is taken into account during all drying operation and the transition between bubbling to slugging regime is delineated for estimating the bubble velocity and size. Such modifications improve the mathematical model to better simulate the drying of coarse particles in fluidized beds. The best estimation of the five adjustable model parameters, which are required to define heat and mass transfer mechanisms between interstitial gas and seed particles and to specify the heat loss from dryer walls to ambient air, is attained by incorporating an optimization routine into the computer model program. Having been specially designed to supply data for this model, experiments are performed in a bath laboratory-scale fluidized bed. Additional data are generated to validate the model and program routines. Results show a good agreement between simulated and experimental data, validating the approach used to describe drying kinetics and particle shrinkage.

Keywords Drying mechanism; Fluidized bed regimes; Three-phase model

INTRODUCTION

Fluidized beds are used industrially for processing solid particles with a mean size diameter varying from 50 μm to 3 mm. Drying particles is commonly performed in such beds because of the efficient contact between gas and solids that allows higher heat and mass transfer coefficients between these phases, inducing great drying rates. Moreover, the intensive gas–solids mixing that occurs due to bubbling regime results in quite uniform temperature and moisture content of solids inside the dryer.[1–3] This assures good drying control for very sensitive materials, such as seeds and grains that need to reduce water activity for improving their shelf life before consumption or germination.

Since the fluidization technique is commonly employed in industrial processes, several fundamental works can be found in the literature, focusing on modeling the solid–gas contact operation. The main difference among these models is concerning to the fluid flow rate representation and the interactions between each phase assumed to exist inside the fluidized bed.

As pointed out by Yates,[4] the two-phase theory formulated in 1952 states that "all gas in excess of that necessary to just fluidize the bed passes through in the form of bubbles." Kunii and Levenspiel[5] have applied this two-phase theory to model different operations in fluidized beds of particles belonging to A and B groups of Geldart classification[6] under freely bubbling regime conditions. Following their model, heat and mass transfer from one phase to another is due to interactions between particles and interstitial gas in the emulsion phase, between interstitial gas and cloud wake in the cloud-emulsion inter-phase, and between cloud wake and bubble in the cloud-bubble inter-phase. However, the serious criticism of this model is the amount of the gas in excess that really forms bubbles.

Zahed et al.[2] have modified this two-phase model to describe the drying of grains (coarse particles) in batch fluidized beds by assuming the diffusive model for mass transfer, the perfectly back-mixed for the emulsion phase behavior, and the plug flow for the bubble phase that is free of particle. Although their model results still need to be validated by experimental data, simulated trends have been consistent with physical expectations and fundamentals.

By considering also two phases, the particle-free bubble and emulsion phases, Groenewold and Tsotsas[7] have reduced the gas fraction that really forms bubbles to model the batch drying operation in fluidized beds of particles belonging to Geldart group D. Although these authors have identified the effect of flow regimes (bed height and gas flow

Correspondence: M. L. Passos, Programa de Pós-Graduação em Engenharia Química, Centro de Secagem de Pastas, Suspensões e Sementes, Universidade Federal de São Carlos, P. O. Box 676, Rod. Washington Luiz, km 235-zip 13565-905, São Carlos, SP, Brazil; E-mail: merilau@task.com.br

rate) on heat and mass transfer mechanisms between particle–gas–bubble, their model does not describe such effect but corrects the emulsion gas flow by introducing an apparent Sherwood number function of the bed height.

For drying particles belonging to Geldart group B, Ciesielczyk[8] has incorporated an adjustable parameter into the model to take into account the presence of solids into the bubble phase. Also, this author has used the concept of a generalized drying curve to include the constant and falling drying rate periods in the model. His model describes the gas flow in the bubbling fluidized bed regime. However, effects of bed height and column diameter on the bubble size are only applied for fine particles belonging to Geldart group B.

Based on a three-phase model, Wildhagen et al.[9] have described the batch drying of porous alumina in a fluidized bed, assuming that solids are perfectly mixed and the bubble phase and the interstitial gas are in plug flow. Solids in the cloud phase as well as the energy loss through the dryer walls have been neglected. Using a three-phase model, Topuz et al.[10] have modeled the grain drying kinetics considering both the constant and falling drying rate periods.

Vitor et al.[11] have modified the Wildhagen et al. model for simulating the drying of biomass powder (group B of Geldart classification) in fluidized beds. These modifications incorporate into the model the energy loss through the column wall, the option of perfect mixing or of plug flow for the interstitial gas in the emulsion phase, and the actual fraction of gas in excess that composes the bubble phase for particles from Geldart group B. This modified model has been expressed by an algebraic-differential equation system, easy to solve since the enthalpy for each phase, expressed as a function of temperature, is formulated as an algebraic model restriction.

To extend this three-phase model for describing the drying of particles belonging to Geldart group D, flow regimes as well as bubble size, shape, and rise in velocity have been analyzed as a function of the particle-to–column size ratio and column characteristics in previous works.[12,13] Incorporating such correlations into the model, the first attempt to simulate heat transfer between bubble–gas–particles in beds of grass seeds (*Brachiaria brizantha*) has been made.[12] Based on these results, the present work aims at modifying this three-phase model for simulating the drying of these seeds in batch fluidized beds, taking into account: (a) transience of heat and mass transfer mechanism; (b) shrinkage of particles as water evaporates; and (c) drying kinetics including both the constant rate and the falling rate.

Experiments carried out in the laboratory-scale fluidized bed unit at three different levels of inlet air temperature and flow rate generate data to determine heat transfer coefficients between solids and interstitial gas and between column walls and air ambient, as well as the drying kinetic constants from this modified three-phase model.

THREE-PHASE MATHEMATICAL MODEL

Basic Assumptions and Model Equations

The three-phase drying model proposed by Vitor et al.[11] assumes that solids are perfectly mixed while bubbles are moving upwards in plug flow through the column. Interstitial gas can flow in perfect mixing or in an arbitrary regime between plug flow and perfect mixing. Furthermore, this interstitial gas is one responsible for the energy lost to ambient air through the column wall.

Mass and energy balance equations for the three-phases are written as follows:

Solid Phase

$$(1-\varepsilon)\rho_s \frac{dY_s}{dt} = -f_{M1T} \tag{1a}$$

$$(1-\varepsilon)\rho_s \frac{dH_{su}}{dt} = f_{E1T} - f_{M1T}(H_u + \lambda_0) \tag{1b}$$

$$H_{su} = H_s + H_u Y_s;\ H_s = c_{ps}(T_s - T_R);\ H_u = c_{pl}(T_s - T_R) \tag{1c}$$

Equations (1a) and (1b) represent, respectively, the mass and energy balances for this solid phase, while Eq. (1c) defines the enthalpy of wet solids, H_{su}, as function of the dry solids enthalpy, H_s, and the water enthalpy, H_u. Note that f_{M1T} and f_{E1T} are, respectively, the mass and heat transfer rates between solid and interstitial gas phases along all bed height per unit of bed volume, as schematized in Table 1.

Interstitial Gas Phase

$$(1-\delta)\varepsilon_{mf}\rho_g \frac{\partial Y_{gi}}{\partial t} + G_{gi}\beta_M \frac{Y_{gi} - Y_{g0}}{L} = f_{M1} - f_{M2} \tag{2a}$$

$$(1-\delta)\varepsilon_{mf}\rho_g \frac{\partial H_i}{\partial t} + G_{gi}\ \beta_T \frac{H_i - H_0}{L} = f_{E2} - f_{E1} + f_{M1}(H_u + \lambda_0) - f_{M2}H_{vi} - E_w \tag{2b}$$

$$H_i = H_{gi} + H_{vi}Y_{gi};\ H_{gi} = c_{pg}(T_{gi} - T_R);\ H_{vi} = \lambda_0 + c_{pv}(T_{gi} - T_R) \tag{2c}$$

Similarly, Eqs. (2a) and (2b) represent, respectively, the mass and energy balances for the interstitial gas phase. Equation (2c) defines the enthalpy of this interstitial gas phase, H_i, as a function of the interstitial dry gas enthalpy, H_{gi}, and the interstitial vapor enthalpy, H_{vi}. Note that f_{M1} and f_{E1} represent the mass and heat transfer rates between solid and interstitial gas phases along an infinitesimal height of bed, dz, per unit of bed volume. Similarly, f_{M2} and f_{E2} represent the mass and heat transfer rates between the interstitial gas phase and the bubble gas phase along an infinitesimal height of bed, dz, per unit of bed volume

TABLE 1
Interactions between phases[11]

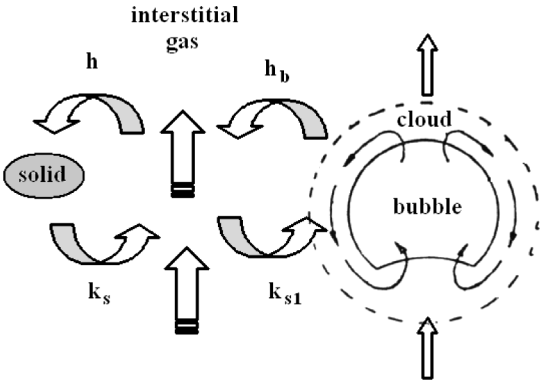

$$f_{E1} = ha(T_{gi} - T_s) \quad f_{M1} = k_s a(Y_s - Y_s^*)$$

$$f_{E2} = h_b a_1(T_{gb} - T_{gi}) \quad f_{M2} = k_{s1} a_1(Y_{gi} - Y_{gb})$$

$$f_{E1T} = \frac{1}{N}\sum_{k=1}^{N} f_{E1}^{(k)} \quad f_{M1T} = \frac{1}{N}\sum_{k=1}^{N} f_{M1}^{(k)}$$

$$f_{E2T} = \frac{1}{N}\sum_{k=1}^{N} f_{E2}^{(k)} \quad f_{M2T} = \frac{1}{N}\sum_{k=1}^{N} f_{M2}^{(k)}$$

with $a = \frac{6(1-\varepsilon_{mf})}{d_p \phi}$

$$h_b a_1 = \frac{(h_{bc}a_b)(h_{cg}a_{gi})}{h_{bc}a_b + h_{cg}a_{gi}}$$

$$\begin{cases} h_{bc}a_b = \delta\left\{4.5\left(\dfrac{G_{mf}c_{pg}}{d_b}\right) + 5.85\left[\dfrac{(k_G c_{pg}\rho_g)^{1/2} g^{1/4}}{d_b^{1,25}}\right]\right\} \\ h_{cg}a_e = \delta\left\{6.78(\rho_g c_{pg} k_g)^{1/2}\left[\dfrac{\varepsilon_{mf} u_b}{d_b^3}\right]^{1/2}\right\} \end{cases}$$

$$k_{s1}a_1 = \frac{(k_{bc}a_b)(k_{cg}a_{gi})}{k_{bc}a_b + k_{cg}a_{gi}}$$

$$\begin{cases} k_{bc}a_b = \delta\rho_g\left\{4.5\left(\dfrac{G_{mf}}{\rho_g d_b}\right) + 5.85\left[\dfrac{(D_{vg})^{1/2} g^{1/4}}{d_b^{1,25}}\right]\right\} \\ k_{cg}a_e = \delta\rho_g 6.78\left[\dfrac{\varepsilon_{mf} D_{vg} u_b}{d_b^3}\right]^{1/2} \end{cases}$$

(see Table 1). Moreover, E_w is the rate of heat lost through the column wall per unit of bed volume.

As shown in the previous work,[12] in Eq. (2a) and Eq. (2b), the β value is dictated by the interstitial gas phase flow regime; i.e.,

- If the interstitial gas moves in plug flow, then: $\beta_M = \left(\frac{L}{Y_{gi}-Y_{g0}}\right)\frac{\partial Y_{gi}(z,t)}{\partial z}$;

$$\beta_T = \left(\frac{L}{H_i - H_0}\right)\frac{\partial H_i(z,t)}{\partial z};$$

- if the interstitial gas is in perfect mixing then $\beta_M = \beta_T = 1$; Y_{gi} and H_i depend on time, t, but not on z;
- if the interstitial gas moves in an arbitrary flow then $1 < \beta_M \leq 1.5$ and $1 < \beta_T \leq 1.5$ (their actual values need to be determined experimentally).

Therefore, unless the interstitial gas flow regime is known, β_M and β_T are adjustable parameters of the model.

Bubble Gas Phase

$$\delta\rho_g \frac{\partial Y_{gb}(z,t)}{\partial t} + G_{gb}\frac{\partial Y_{gb}(z,t)}{\partial z} = f_{M2} \tag{3a}$$

$$\delta\rho_g \frac{\partial H_b(z,t)}{\partial t} + G_{gb}\frac{\partial H_b(z,t)}{\partial z} = f_{M2}\ H_{vi} - f_{E2} \tag{3b}$$

$$H_b = H_{gb} + H_{vb}Y_{gb};\ H_{gb} = c_{pg}(T_{gb} - T_R);\quad H_{vb} = \lambda_0 + c_{pv}(T_{gb} - T_R) \tag{3c}$$

Equations (3a) and (3b) represent, respectively, the mass and energy balances for the bubble gas phase. Equation (3c) defines the enthalpy of this bubble gas phase, H_b, as a function of the bubble dry gas enthalpy, H_{gb}, and the bubble vapor enthalpy, H_{vb}. This bubble gas phase moves in plug flow, meaning that $Y_{gb} = Y_{gb}(z,t)$ and $H_b = H_b(z,t)$

Table 1 schematizes interactions between these three phases. Heat and mass transfer coefficients between gas interstitial and bubble (h_b and K_{s1}, respectively) are

estimated from correlations proposed by Kunii and Levenspiel,[5] as shown in Table 1.

In addition, the rate of heat lost through the column wall per unit of bed volume, E_w, is expressed as:

$$E_w = \alpha_w \frac{A_L}{V_{bed}}(T_g^M - T_a) = \alpha_{wa} \frac{A_L}{V_{bed}}(T_w^M - T_a) \qquad (4)$$

Modifications Model

Fluid Flow

Based on previous works,[12,13] one can see in Table 2 that gas flows quite differently in fluidized beds of group D particles than it flows in fluidized beds of group B particles.

Moreover, the gas flow is divided over the bubble phase and the interstitial or dense phase as:

$$G_{gb} = \Psi(G_g - G_{mf}) = \rho_g \Psi(U_g - U_{mf}) \qquad (5)$$

with $\Psi = 1$ according to the two-phase theory. However, as pointed out by Yates,[4] there is a deviation from this theory since Ψ actually decreases as the particle diameter increases. As shown in the previous work[12] for coarse particles belonging to Geldart group D, Ψ equals to 0.26 under the bubbling regime and to 1 under the continuously slugging regime.

Equation (6) and correlations presented in Table 2 for particles from group D have already been incorporated into the model for better describing the gas flow in fluidized

TABLE 2
Flow regime correlations for particles belonging to Geldart group B and D[12]

Flow parameters	Group B	Group D
Geldart classification diagram 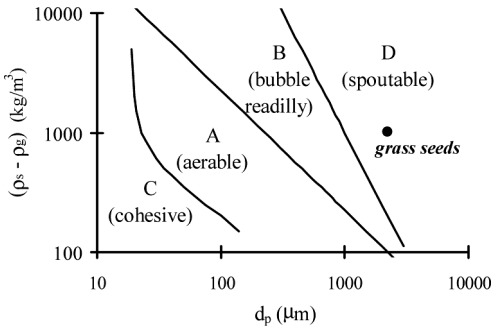	Fluidization: normal $U_{mb}/U_{mf} < 1$ Bed expansion: moderate, increasing with (U_g/U_{mf}) Bubble velocity: fast $u_b \geq (U_{mf}/\varepsilon_{mf})$ Bubble shape: rounded (small indentation) Bubble mixing: bubble induced drift + wake Type of slug: 	Fluidization: unstable $U_{mb}/U_{mf} = 1$ Bed expansion: low (just after onset of bubbling) Bubble shape: rounded (small wakes) Bubble velocity slow: $u_b < (U_{mf}/\varepsilon_{mf})$ Bubble-induced drift Type of slug: 
Bubble diameter: $d_b = \left(\frac{6V_{bubble}}{\pi}\right)^{1/3}$	d_b expressed as a function of $(U_g - U_{mf})$; distributor design and axial distance z.	$d_b = 2.25z^{0.81}(U - U_{mb})^{1.11}$
Bubble or slug rise velocity:		
Bubbling regime: $u_b = f_w(c_1\sqrt{g}d_b)$ $u_a = (U_g - U_{mf}) + u_b$		
Geldart: group B $\Rightarrow c_1 = 0.50$ group D $\Rightarrow c_1 = 0.71$		
for $d_b/D_c < 0.125 \Rightarrow f_w = 1$ and for $0.125 \leq d_b/D_c \leq 0.6 \Rightarrow f_w = 1.13\ \exp\left(\frac{d_b}{D_c}\right)$		
Continuously slugging regime (if $d_b/D_c > 0.6$):	$u_b = 0.35(\sqrt{gd_b})$ $u_a = (U_g - U_{mf}) + u_b$	
Bed porosity and bubble concentration:		
$\varepsilon_{mf} = 1.0 - \frac{4M_s}{\rho_s \pi D_c^2 L_{mf}}$; $\quad \delta = 1.0 - \frac{L_{mf}}{L} = \frac{\Psi(U_g - U_{mf})}{u_a}$		

L_{mf}: bed height at minimum fluidization; L: expanded bed height; ε_{mf}: bed porosity at minimum fluidization; δ: volumetric bubble gas phase concentration; Ψ: ratio of the visible bubble flow to the excess gas velocity.

bed of these particles.[12] In the computational program developed for solving the modified model, the wall effect on the bubble rise velocity is taken as a restriction even when $d_b/D_c > 0.125$. Moreover, the axial distance z, at which the transition between bubbling and slugging regimes occurs, is determined previously (taking $d_b = 0.6\ D_c$; see Table 2) in order to establish the flow regime along the bed height. This information is fundamental to estimate the volumetric bubble concentration (δ) and the volumetric heat and mass transfer coefficients between cloud and interstitial gas, which depend on the bubble or slug velocity, as one can see in Table 1.

Note that, in the laboratory-scale fluidized bed unit, wall effects and changes in the fluid flow regime can strongly affect the heat and mass transfer mechanisms.

Heat Transfer Mechanism

To uncouple E_w from the gas temperature, the wall heat transfer coefficient, α_{wa} in Eq. (4), has been chosen as the one adjustable parameter of this modified model.[12] Therefore, the mean column wall temperature should be measured during the experiments. Under the fluidized bed design condition, this wall temperature can be fitted by choosing the appropriate material to build the column. Register that Victor et al.[11] used α_w (the overall heat transfer coefficient) as the model parameter to calculate E_w.

By using air as the drying agent, the heat transfer coefficient between particle and interstitial gas, h, can be simplified as a function of $\mathrm{Re}_p = G_{gi} \cdot d_p/\mu_g i$ (Reynolds number of particle for the interstitial gas phase):

$$h = \frac{k_{gi}}{d_p}(x_1 \mathrm{Re}_p^{x_2}) \tag{6}$$

In Eq. (6), x_1 and x_2 are the two adjustable model parameters concerning the particle–gas heat transfer mechanism.

Drying Kinetic Equations

As shown in Fig. 1, the characteristic drying curve of grass seeds clearly presents two mechanisms, the first in which the seed moisture content varies linearly with time (constant drying rate) and the second in which the seed moisture content decreases exponentially with time (falling drying rate).

Since water evaporates from the wet surface of grass and transfers to the interstitial gas in the first drying period, the mass transfer coefficient between particle and interstitial gas depends strongly on gas flow characteristics, expressed by Reynolds number. Therefore, the following equation is proposed for describing this first drying mechanism, as corroborated in Fig. 1:

for $Y_s \geq Y_{scr}$:

$$\frac{Y_s - Y_s^*}{Y_{s0} - Y_s^*} = 1 - k_I\ t \Rightarrow \frac{dY_s}{dt} = -k_I(Y_{s0} - Y_s^*) \tag{7a}$$

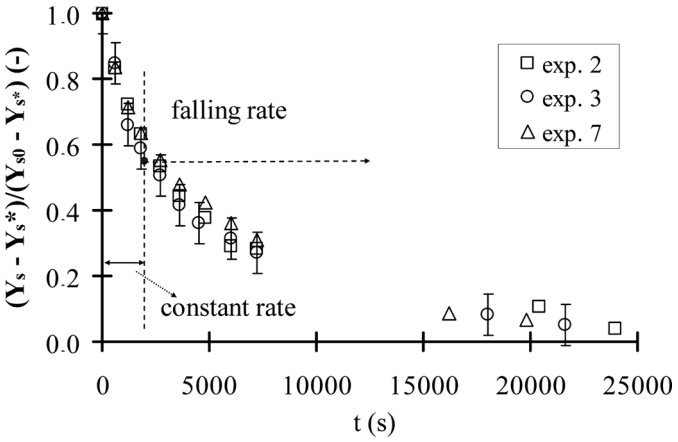

FIG. 1. Typical drying curves of grass seeds in the fluidized bed (data from tests 2, 3, and 7, presented in Table 4).

This first period extents until the particle moisture content achieves its critical value, $Y_s = Y_{scr}$. Just below this value, the drying rate starts falling with time. Thus, for $Y_s \geq Y_{scr}$, Eq. (7b) is the one used in the model to calculate f_{M1T}. The x_{11} and x_{21} are the two adjustable model parameters for this first period.

$$f_{M1T} = k_s a(Y_s - Y_s^*)$$

$$with\colon\ Y_s \geq Y_{scr}$$

$$k_s a = (1-\varepsilon)\rho_s k_I \frac{(Y_{s0} - Y_s^*)}{(Y_s - Y_s^*)}$$

$$k_I = \left(\frac{D_{vi}}{d_p}\right) x_{1I} \mathrm{Re}_p^{x_{2I}} \tag{7b}$$

The second drying period is formulated considering the diffusion model associated to the particle shrinking. Following Reyes et al.,[14] drying kinetics of agricultural materials, which undergo significant volume contractions during the falling period, can be described using the one modified Fick's correlation, which incorporates an effective water diffusivity and the particle size variation. Based also on extensive works of Becker[15] and Lewis,[16] the following approach is used to describe drying kinetics in the falling rate period in which $Y_{scr} \geq Y_s \geq Y_s^*$:

for $Y_s^* \leq Y_s \leq Y_{scr}$:

$$\frac{Y_s - Y_s^*}{Y_{s0} - Y_s^*} = k_{II} \exp\left(\frac{-D_{ef}\, t}{(d_p \phi/6)^2}\right) \tag{8a}$$

or

$$\frac{dY_s}{dt} \cong \left(\frac{Y_s - Y_s^*}{Y_{s0} - Y_s^*}\right)\left(\frac{-D_{ef}}{(d_p\phi/6)^2}\right)(Y_{s0} - Y_s^*)$$

Based on Eq. (8a), f_{M1T} is calculated for the second period of drying as:

$$f_{M1T} = k_s a\left(Y_s - Y_s^*\right)$$
$$\text{with: } Y_{scr} \geq Y_s \geq Y_s^*$$
$$k_s a = (1-\varepsilon)\rho_s\left(\frac{36 \times D_{ef}}{\left(d_p\phi\right)^2}\right)$$
$$D_{ef} = x_{1II}\exp\left(\frac{-x_{2II}}{T_s}\right) \tag{8b}$$

For the falling drying rate period, x_{1II} and x_{2II} are the two adjustable model parameters to be determined. Although these two parameters replace x_{1I} and x_{2I} as $Y_s \leq Y_{scr}$, they are interlinked since their values depend on the x_{1I} and x_{2I} determination for the continuity of the drying curve.

Numerical Method to Solve the Model

Based on Eqs. (1)–(8), five adjustable parameters, x_1, x_2, x_{1I} (or x_{1II}), x_{2I} (or x_{2II}), and α_{wa}, must be estimated when the flow regime of the interstitial gas phase is already known. This model parameter estimation is performed using experimental data together with the model solution.

The DASSL computational code[17] has been chosen to solve this system of differential-algebraic equations (Eqs. (1) to (3)) after discretization of the z spatial coordinate.

The initial and boundary conditions for solving these model equations are given by Eq. (9):

$$\begin{aligned} Y_s(0) &= Y_{s0} \\ Y_{gi}(0,z) &= Y_{gb}(0,z) = Y_{g0} \\ Y_{gi}(t,0) &= Y_{gb}(t,0) = Y_{g0}^* \\ &\quad + (Y_{g0} - y_0^*)[1-\exp(-t/\tau)], \quad \text{with } \tau \leq 0.1\,\text{s} \end{aligned} \tag{9}$$

Y_{g0}^* is absolute gas humidity in equilibrium with Y_{s0}.

$$\begin{aligned} T_{gi}(0,z) &= T_{gb}(0,z) = T_{s0} \\ T_{gi}(t,0) &= T_{gb}(t,0) = T_{s0} \\ &\quad + (T_{g0} - T_{s0})[1-\exp(-t/\tau)], \quad \text{with } \tau \leq 0.1\,\text{s}, \end{aligned}$$

These input variables, as well as the particle properties (see Table 3 must be supplied to the computer program. The mean output variables from the computer model program are the particle temperature and moisture content during the drying time and the outlet gas temperature

TABLE 3
Properties of the grass seeds and experimental techniques employed

Particle properties	Experimental techniques
Density (at $Y_s = 0.063$): ρ_s (kg/m^3) $= 1018 \pm 20$	Pycnometry with ether
Size: L_1 (m) $= 3.61 \times 10^{-3}$; L_2 (m) $= 1.86 \times 10^{-3}$	Direct measurements of three (L_1, L_2, and L_3) dimensions at different levels of moisture content[20]
L_3 (m) $= 1.5 \times 10^{-3} + 2.67 \times 10^{-3}\left(\frac{Y_s}{1+Y_s}\right)$	
$V_p = 5.35 \times 10^{-9} + 9.44 \times 10^{-9}\left(\frac{Y_s}{1+Y_s}\right)$	Geometric particle shape for volume (V_p) and surface area (S_p) calculations: prolate spheroid with semi-axes: $L_1/2$ and $(L_2+L_3)/4$.
$d_p = \left[V_p \frac{6}{\pi}\right]^{1/3}$; $\phi = \frac{\pi d_p^2}{S_p}$	
Mean specific heat (at $0.098 < Y_s < 0.174$)	Differential scanning calorimetry (DSC)
c_{ps} (J/kg K) $= 428$	
Minimum fluidization condition: G_{mf} (kg/m^{2}s) $= 0.682$	Pressure drop vs. air flow rate curves with direct measurements of bed height
ε_{mf} $(-) = 0.392$	
Sorptium curve described by the Haslsey modified equation: $Y_s^* = (0.668 - 0.0019T)(-lnRH)^{-0.14}$	Dynamic equilibrium (injecting a controlled air into the bed of grass seeds measuring the moisture content until reaching a constant value)
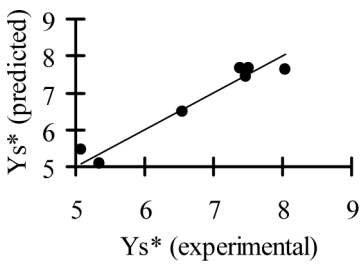	The best correlation to fit data obtained from statistical analysis (standard deviation between experimental and predicted data = 0.0035; error between model and experiments: 0.0037)
Critical moisture content: $Y_{scr} = 0.140 \pm 0.001$	considering constant within the range used for performed the drying tests (see Table 4)

and humidity. These two latter variables, which can be measured during experiments, are obtained by well-mixing the interstitial gas phase with the bubble gas phase as:

$$Y_{gL} = \frac{G_{gi} Y_{gi|z=L} + G_{gb} Y_{gb|z=L}}{G_g}$$
$$H_{gL} = \frac{\left[G_{gi} H_g\right]_{z=L} + \left[G_{gb} H_{gb}\right]_{z=L}}{G_g} \quad (10)$$

The parameter estimation procedure comprises: (a) the heuristic method of PSO optimization[18] to locate the rough solution and (b) the maximum likelihood method of ESTIMA computational code[19] to refine the rough solution. The objective function defined in this optimization problem (one to be minimized for assuring the best values of the five adjustable parameters) is:

$$f_{obj} = \sum_{1}^{56} \sum_{1}^{4} \frac{\left(vout_{i_{|sim}} - vout_{i_{|\exp}}\right)^2}{\sigma_{i\exp}} \quad (11)$$

with $vout_i$ representing one of the four output variables (i varies from 1 to 4 variables; i.e., T_s, Y_s, T_{gL}, and Y_{gL}) and $\sigma_{i\exp}$ its variance calculated from data replication at the central point.

EXPERIMENTAL METHODOLOGY

Grass seeds of *Brachiaria brizantha* are used to perform the mass transfer tests. Their physical properties are shown in Table 3. As noted, these seeds belong to Geldart group D with the flow regime behavior described in Table 2. As shown by Arnosti et al.,[20] since the seed size (L_3; see Table 3) depends on the moisture content, during drying, the seed volume and surface shrink (V_p and S_p; see Table 3). Therefore, the volume-to-surface ratio $V_p/S_p = d_p\ \phi$ is reduced as the seed moisture content decreases. Based on the correlations of Arnosti et al. presented in Table 3, the V_p/S_p ratio ($=d_p\ \phi$) can be calculated during the drying operation. Figure 2 shows the typical V_p/S_p decay curve, predicted by the correlations of Arnosti et al.,[20] during drying operation in the fluidized bed.

Figure 3 schematizes the experimental setup used during tests. The laboratory-scale column has 0.07 m of diameter and 0.40 m of height. It is built in glass to allow visual observation of fluid flow regimes. Air is drawn by a centrifugal fan inserted into a closet cabinet at the bottom of the column. This air passes through a mesh filter, a 2-kW electrical heater, and a mesh plate distributor before fluidizing the bed of particles. After leaving the column, the exit air passes through a calibrated orifice plate for registering its flow rate. As shown in Fig. 3, a water manometer is used to measure the actually pressure drop across the bed. A valve, located inside the cabinet, controls the airflow rate. This lab-scale column has been selected first to better analyze drying kinetics due to the easier control

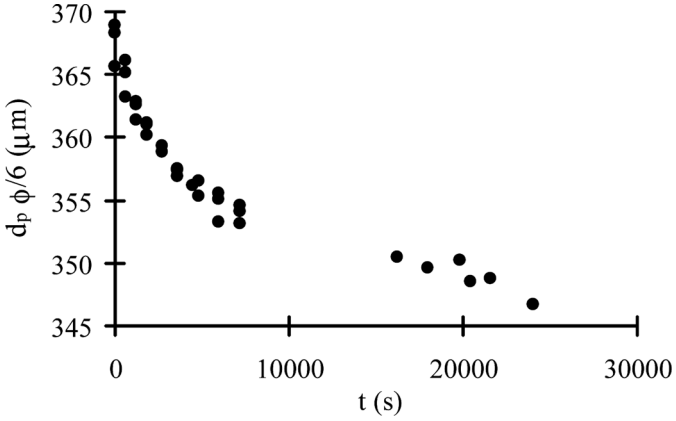

FIG. 2. Shrinkage of grass seeds during the typical drying test, following correlations proposed by Arnosti et al.[20] and presented in Table 3. (Seed moisture content data obtained from tests 2, 3, and 7).

of the operational variables. Further studies should be performed in a pilot-scale column.

Three copper-constantan thermocouples are installed inside the column to measure (see Fig. 3): the inlet air temperature, T_{g0} (thermocouple inserted just before the distributor plate); the solid–gas emulsion temperature, T_{bed}, or the solid temperature, T_s (thermocouple placed 0.10 m above the air distributor); and the outlet air temperature, T_{gL} (thermocouple placed at $z = 0.38$ m from the base of the column). The solid temperature, T_s, is measured during a short time interval at which the bed is collapsed; details of this method are discussed by Rizzi et al.[13] A thermocouple adhered to the outer column wall (at $z = 0.10$ m) records the column wall temperature, T_w. Another thermocouple, located close to the experimental unit, registers the ambient temperature for each experiment. A laboratory humidity

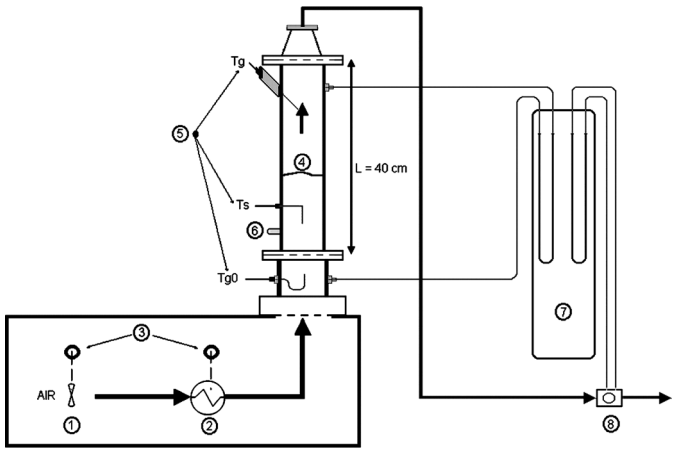

FIG. 3. Experimental setup: ① air blower; ② electrical heater; ③ gas flow rate and temperature controls; ④ glass column; ⑤ thermocouples connected to a digital temperature recorder; ⑥ samples withdrawal; ⑦ water manometers; and orifice plate.

TABLE 4
Operational conditions of experiments

Test #	G_g (kg m^{-2}s^{-1})	T_{g0}(°C)	T_{s0}(°C)	T_a (°C)	T_s^M (°C)	L (m)	Y_{s0} (d.b.)	Y_{g0} (d.b)
1	1.202	51.5	27.6	24.8	34.7	0.226	0.186	0.010
2	1.081	40.9	28.2	25.0	29.3	0.192	0.191	0.009
3	1.092	40.8	30.2	22.3	28.8	0.206	0.195	0.010
4	0.949	35.3	30.3	25.2	27.5	0.178	0.199	0.012
5	0.925	51.5	31.5	26.6	33.5	0.175	0.222	0.012
6	1.227	37.2	29.9	25.4	28.6	0.221	0.178	0.012
7	1.100	41.5	16.9	20.7	26.5	0.210	0.173	0.012
8	1.227	31.5	13.9	22.6	19.8	0.243	0.206	0.008

indicator measures the inlet air humidity. The outlet air humidity is measured by a psychrometer inserted at the air exit. However, due to the transient regime, the outlet air humidity measurements cannot be accurate. Generally, instruments for measuring air humidity require a measure-response time longer than one demand by the process transience.

The solid moisture content, Y_s, is determined during each experiment by sampling seeds from bed and measuring their mass in wet and dry conditions, following the oven method procedure (drying seeds 24 h in the oven at 105.0°C ± 3.0°C) in agreement to the Seed Testing Association Norms (ISTA). To minimize experimental errors, the mass of wet seed samples is settled at 3.0×10^{-3} kg. This value represents a compromise between two errors, one associated with the accuracy of the analytical balance used (Metter Digital with accuracy of 1.0×10^{-6} kg) and the other associated with disturbances in the fluidized bed regime induced by withdrawing samples.

Experimental Procedure

Drying experiments are performed following the factorial design in two levels of the inlet air temperature, T_{g0}, and the airflow rate, G_g, as shown in Table 4.

TABLE 5
Best values of adjustable model parameters and their correlations

Model parameters	Values	Model parameters	Values
x_1	0.630		
x_2	0.275		
x_{1I}	1.1×10^{-3}	x_{1II} (m^2/s)	5.71×10^{-5}
x_{2I}	0.644	x_{2II} (K)	4596.63
α_{wa} (kW/m^{2}K)	3.52		

Constitutive correlations for:

Heat transfer between particle and gas interstitial:

$$Nu = 0.630\ \mathrm{Re}_p^{0.275} \tag{12}$$

Mass transfer between particle and gas interstitial in the first period of drying:

$$\frac{k_I d_p}{D_{vi}} = 1.1 \times 10^{-3} \mathrm{Re}_p^{0.644} \tag{13}$$

Mass transfer between particle and gas interstitial in the second period of drying:

$$D_{ef} = 5.71 \times 10^{-5} \exp\left(-\frac{4596.63}{T_s}\right) \tag{14}$$

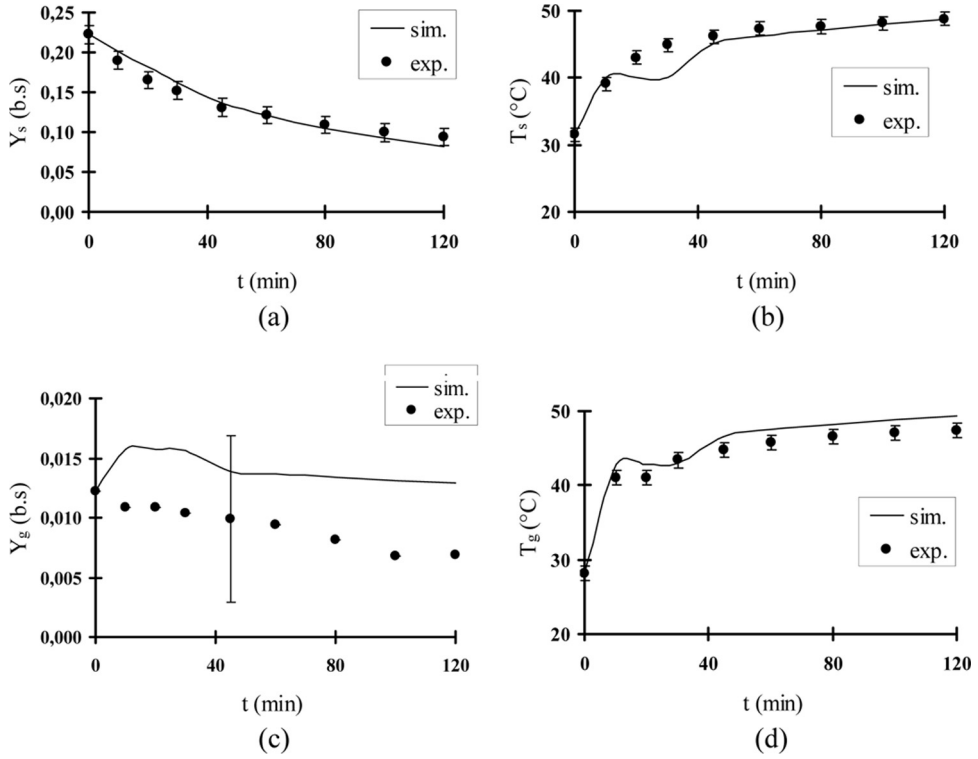

FIG. 4. The best fit of the proposed model to experimental data: (a) drying curve; (b) seed temperature; (c) outlet air humidity and (d) outlet air temperature. (Data from test 5; other tests presents similar trends).

Three replications at the central point (tests 2, 3, and 7) are used to evaluate data replication and experimental errors.

In all these tests, the mass of grass seeds is settled at 0.400 kg. The initial moisture content, Y_{s0}, and particle temperature, T_{s0}, are given in Table 4. Values of T_w^M and T_a are averaged over, at least, 11 measurements performed during each test. The mean error concerning the assumption of taking T_w^M and T_a constant is estimated to be 2.2 and 1.8°C, respectively. It is around two times higher than the experimental error due to temperature measurements.

For each one experiment shown in Table 4, eight sets of data are generated during 120 min of test. Therefore, 56 experimental points are obtained to determine the five adjustable parameters.

In addition, Table 4 presents the eighth experiment that generates the data sets to be used in validating the model.

RESULTS AND DISCUSSION

As shown in earlier works,[12,13] fluidizing grass seeds of *Brachiaria brizantha* by air in this laboratory-scale column favors the development of slugs just after the minimum fluidization condition. From Table 1 one can see that slugs formed in this column tend to be flat; i.e., square-nosed or plug slugs. Such slugs, as observed during the experiments, induce a plug flow regime in the gas phase with particles rain through them rather than moving around.[13]

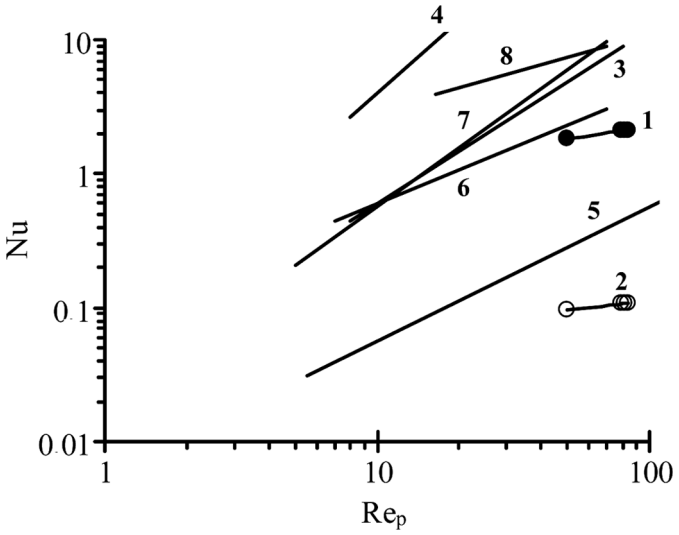

FIG. 5. Nu number as a function of Re_p number for determining the heat transfer coefficient between particles and interstitial gas phase in fluidized beds. Legend: **1**, this work (Eq. (12) in Table 5); **2**, previous correlation;[12] **3**, Frantz correlation;[21] **4**, Leva correlation;[21] **5**, Shin-Jan-Fou et al. correlation;[21] **6**, Lykov correlation;[21] **7**, Zabrodski correlation;[21] **8**, Jun-Chin-Chu correlation.[21]

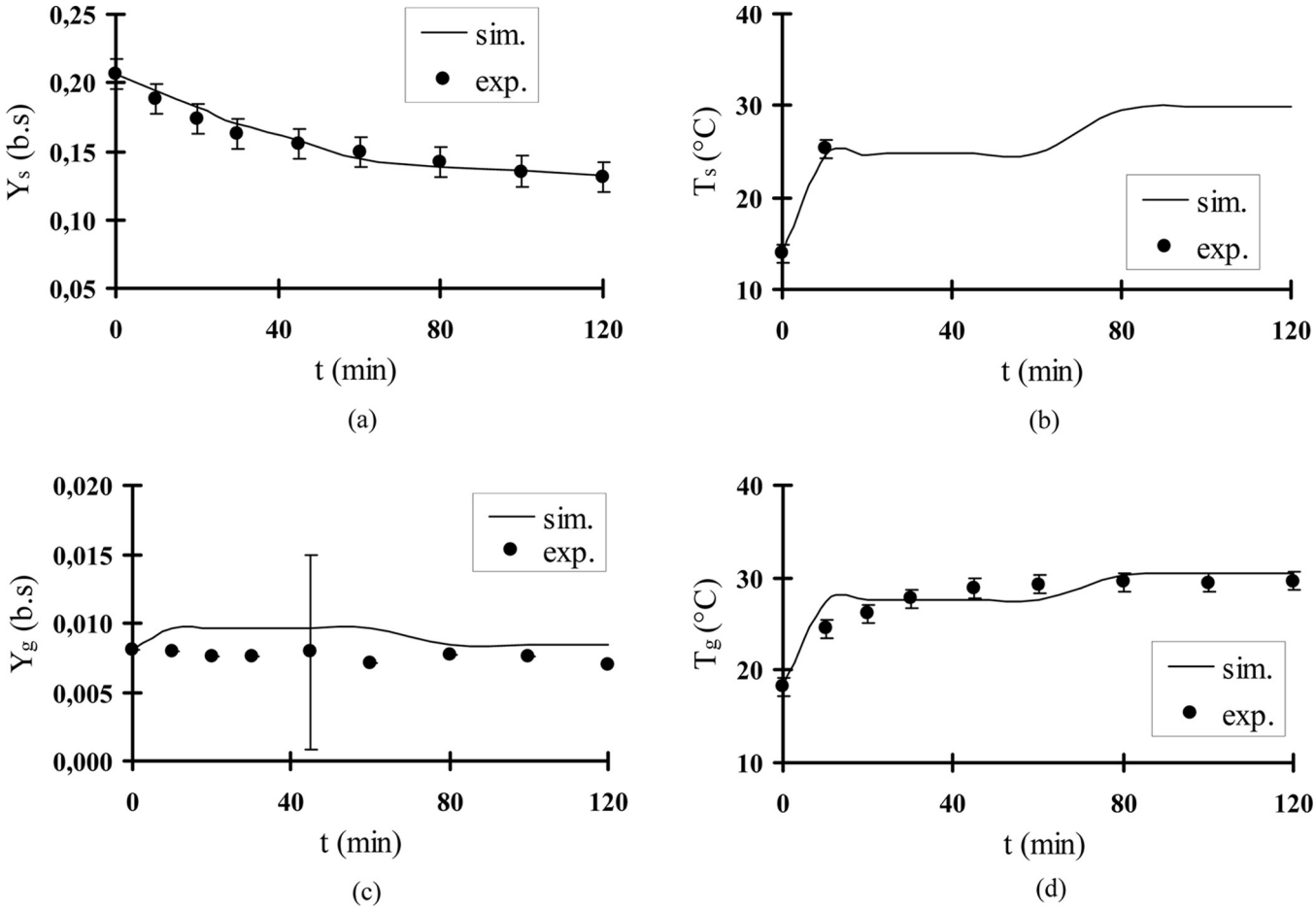

FIG. 6. Comparison between simulated and experimental data: (a) drying curve; (b) seed temperature; (c) outlet air humidity and (d) outlet air temperature (test 8; see Table 4).

Therefore, the present work considers that the interstitial gas phase is in plug-flow regime; i.e.,

$$\beta_M = \left(\frac{L}{Y_{gi} - Y_{g0}}\right)\frac{\partial Y_{gi}(z,t)}{\partial z};\ \beta_{\mathrm{T}} = \left(\frac{L}{H_i - H_0}\right)\frac{\partial H_i(z,t)}{\partial z}$$

in Eq. (2a) and Eq. (2b). Additionally, the continuously slugging regime starts at $d_b/D_c = 0.6$ with all air in excess $(U_g - U_{mf})$ going into slugs; i.e., $\psi = 1$ in Eq. (5).

Table 5 shows the optimum values of the five adjustable model parameters for describing heat and mass transfer mechanisms between grass seeds and air interstitial during the drying operation in fluidized beds as well as the empirical correlations obtained.

Before analyzing the performance of the model in predicting the grass seed drying, data in Fig. 4 corroborate that this modified three-phase model can well fit data to best optimize the values of its five adjustable parameters. As shown in Fig. 4, the model fitting is settled within the range of the experimental error, which is indicated in Fig. 4 by the bar line. As expected, for the outlet air humidity, Y_{gL}, the experimental error, obtained by three replications in the central point (tests 2, 3, and 7), is higher because of the instrumental limitation in measuring transient values of Y_{gL} $(= Y_g$ in Fig. 4).

Although the experimental range of Re_p is already narrow, values of Nusselt, N_u, obtained from Eq. (12) (see Table 4) are compared to those reported in the literature, as shown in Fig. 5. This is a good sign concerning the functionality of this modified three-phase model proposed to predict the heat transfer mechanism between particles and air interstitial.

The correlation obtained for describing the mass transfer between particles and gas interstitial, expressed by Eq. (13) in Table 4, needs to be rewritten regarding the gas concentration gradient to be compared to those reported in the literature. Note that the driving force of vapor–water mass transfer is expressed by the moisture content gradient in the solid phase instead of the vapor concentration gradient in

gas phase (see Eq. (7a)). Equation (14) is one specific to grass seeds since this involves the vapor–water diffusion inside the solid surface.

By incorporating Eqs. (12) to (14) into the model, the computer model program could be run to simulate the drying operation conditions obtained in test 8 (see Table 4). In Fig. 6, simulated data are compared to experimental data. Although operation conditions are quite different from other experiments, simulated data of Y_s and Y_{gL} ($= Y_g$ in Fig. 6) agree quite well with the experimental data within the 95% confidence range, based on the experimental error (indicates by the bar lines). Simulated data of T_{gL} ($= T_g$ in Fig. 6) agree to experimental data within 95% confidence for an experimental error of 2°C equivalent to that obtained by considering the wall and ambient temperature constants.

CONCLUSION

A modified version of the three-phase model is developed in this work to incorporate two different drying kinetics mechanisms in order to describe the constant and the falling rate periods. Moreover, this modified version includes also the effect of particle shrinking into drying kinetics and flow dynamics.

Based on the results, this modified version model simulates well the drying of grass seeds in laboratory-scale fluidized beds, where the continuously slugging regime governs the interstitial gas phase flow. These results validate the approach used to describe drying kinetics and particle shrinkage.

Improvements in this model can be performed by applying it for pilot-scale fluidized beds of different particles belonging to Geldart group D. Following this goal, experimental works are already in development.

ACKNOWLEDGMENTS

The authors thank CAPES for the Ph.D. scholarship of A.C. Rizzi, Jr., and Dr. J.F.A. Vitor for the free copies of the model compute programs.

NOMENCLATURE

A_L	Lateral area of the bed column $= \pi D_c L$ (m^2)
a	Specific exchange superficial area between gas and particles (m^{-1})
c_p	Specific heat ($m^2\ s^{-2}\ K^{-1}$)
c_1	Parameter dependent on particle size, specified in Table 1
D_c	Column diameter (m)
D_{ef}	Effective moisture diffusivity (m^2/s)
D_{vi}	Diffusion coefficient of vapor into air (m^2/s)
d	Diameter (m)
E_w	Rate of energy loss through column wall per unit of bed volume (kJ $s^{-1}\ m^{-3}$)
f_{E1}	Rate of heat transfer between solid–interstitial gas along dz per unit of bed volume (kJ $s^{-1}\ m^{-3}$)
f_{E2}	Rate of heat transfer between interstitial gas and bubbles along dz per unit of bed volume (kJ $s^{-1}\ m^{-3}$)
f_{E1T}	Rate of heat transfer between solid–interstitial gas along all bed height per unit of bed volume (kJ $s^{-1}\ m^{-3}$)
f_{M1}	Rate of mass transfer between solid–interstitial gas along dz per unit of bed volume (kg $s^{-1}\ m^{-3}$)
f_{M2}	Rate of mass transfer between interstitial gas and bubbles along dz per unit of bed volume (kg $s^{-1}\ m^{-3}$)
f_{M1T}	Rate of mass transfer between solid–interstitial gas along all bed height per unit of bed volume (kg $s^{-1}\ m^{-3}$)
f_w	Wall effect factor defined in Table 2
G	Air mass flow rate per cross sectional area of the column (kg $m^{-2}\ s^{-1}$)
H	Specific enthalpy ($m^2\ s^{-2}$)
H_{col}	Height of the column (m)
h	Effective heat transfer coefficient between solid and interstitial gas phase [kg s^{-3} $(°C)^{-1}$]
$h_b a_1$	Volumetric heat transfer coefficient between bubble and interstitial gas phase [kg $m^{-1}\ s^{-3}$ $(°C)^{-1}$]
k_g	Thermal condutivity of gas (kg s^{-3})
k_I	Parameter defined in Eq. (7a) (s^{-1})
k_s	Effective mass transfer coefficient between solid and interstitial gas phase (kg $m^{-2}\ s^{-1}$)
$k_{s1} a_1$	Volumetric mass transfer coefficient between bubble and interstitial gas phase (kg $m^{-3}\ s^{-1}$)
L	Expanded bed height (m)
RH	Relative air humidity (% or $-$)
S	Superficial particle area (m^2)
T	Temperature (°C or K)
T_R	Reference temperature, $= 273.15$ K
T_g^M	Mean gas temperature along the bed height (enthalpy balance for the bubble and interstitial gas mixture (°C or K)
t	Time (s)
U	Superficial gas velocity (m/s)
u_a	Mean bubble or slug velocity (m/s)
u_b	Rise velocity of an isolated bubble or slug (m/s)
V	Volume (m^3)
V_B	Bed volume $= \pi Dc^2\ L/4$ (m^3)
x_1	Adjustable model parameter, defined in Eq. (6)
x_2	Adjustable model parameter, defined in Eq. (6)
$x_{1\mathrm{I}}$	Adjustable model parameter, defined in Eq. (7b)
$x_{2\mathrm{I}}$	Adjustable model parameter, defined in Eq. (7b)
$x_{1\mathrm{II}}$	Adjustable model parameter, defined in Eq. (8b) (m^2/s)
$x_{2\mathrm{II}}$	Adjustable model parameter, defined in Eq. (8b) (K)
Y	Water content in dry basis

Y^*	Equilibrium moisture content
Y_{scr}	Critical moisture content
z	Axial coordinate (m)

Greek Symbols

α_w	Heat transfer coefficient between column walls and air ambient [kJ $s^{-1}m^{-2}$ $(°C)^{-1}$]
δ	Volumetric bubble concentration
ε	Bed porosity
λ	Heat of vaporization at T_R (kJ kg^{-1})
μ	Viscosity (kg s^{-1} m^{-1})
ρ	Density (kg m^{-3})
ϕ	Particle sphericity

Subscripts

0	Initial value
a	Ambient
b	Bubble
bed	Bed
exp	Experimental
g	Gas
i	Interstitial gas
l	Liquid water
m	Gas–solid mixture
mb	Minimum bubbling condition
mf	Minimum fluidization condition
out	Outlet
p	Particle
s	Solid
v	Vapor water
w	Wall

Superscripts

M	Mean value

Dimensionless Numbers

Nu	Nusselt number $(=h.d_p/k_{gi})$
Re_p	Reynolds number of particle $(=G_{gi}.d_p/\mu_{gi})$

REFERENCES

1. Chandran, A.N.; Rao, S.S.; Varma, Y.B.G. Fluidised bed drying of solids. AIChE Journal **1990**, *36* (1), 29–38.
2. Zahed, A.H.; Zhu, J.X.; Grace, J.R. Modelling and simulation of batch and continuous fluidized bed dryers. Drying Technology **1995**, *13* (1–2), 1–28.
3. Wang, Z.H.; Chen, G. Heat and mass transfer in batch fluidized-bed drying of porous particles. Chemical Engineering Science **2000**, *55* (10), 1857–69.
4. Yates, J.G. *Fundamental of Fluidized-bed Chemical Processes*; Butterworths: London, 1983.
5. Kunii, D.; Levenspiel, O. *Fluidization Engineering*; John Wiley & Sons: New York, 1969.
6. Geldart, D. *Gas Fluidization Technology*; John Wiley & Sons: New York, 1986.
7. Groenewold, H.; Tsotsas, E. A new model for fluid bed drying. Drying Technology **1997**, *15* (6–8), 1687–1698.
8. Ciesielczyk, W. Batch drying kinetics in a two-zone bubbling fluidized bed. Drying Technology **2005**, *23*, 1613–1640.
9. Wildhagen, G.R.S.; Calçada, L.A.; Massarani, G. Drying of porous particles in fluidized beds: Modeling and experiments. Journal of Porous Media **2002**, *5* (2), 123–133.
10. Topuz, A.; Gur, M.; Gul, M.Z. An experimental and numerical study of fluidized bed drying of hazelnuts. Applied Thermal Engineering **2004**, *24*, 1535–1547.
11. Vitor, J.F.A.; Biscaia Jr., E.C.; Massarani, G. Modeling of biomass drying in fluidized bed. Proceedings of the 14th International Drying Symposium (IDS 2004), São Paulo-SP, August, 22–25, 2004; CD-ROM:1104–11.
12. Rizzi Jr., A.C.; Passos, M.L.; Freire, J.T. Modeling and simulating the drying of grass seeds in fluidized beds: Evaluation of heat transfer coefficients. Brazilian Journal of Chemical Engineering **2007** (in press).
13. Rizzi Jr., A.C.; Passos, M.L.; Freire, J.T. Drying of grass seeds (*Brachiaria brizantha*) in fluidized bed. Part I: Preliminary studies. Proceedings of the 31st Brazilian Congress of Particulate Systems (XXXI ENEMP), Uberlândia-MG, October 24–27, 2004 (in Portuguese).
14. Reyes, A.; Alvarez, P.I.; Marquardt, F.H. Drying of carrots in a fluidized bed. I. Effects of drying conditions and modeling. Drying Technology **2002**, *20* (7), 1463–1483.
15. Becker, H. A study of diffusion in solids of arbitrary shape with application to the drying of wheat kernel. Journal of Applied Polymer Science **1959**, *1*, 212–226.
16. Lewis, W.K. The rate of drying of solid materials. Industrial and Engineering Chemistry **1921**, *13*, 427–432.
17. Petzold, L.R. *DASSL: A Differential-Algebraic System Solver*; Computer and Mathematical Research Division, Lawrence Livermore National Laboratory: Livermore, CA, 1989.
18. Kennedy, J.; Eberhart, R.C. Particle swarm optimization. In *Proceedings of the IEEE International Conference of Neural Networks*; Perth, Western Australia, November 27–December 1, 1995; 1942–1948.
19. Noronha, F.B.; Pinto, J.C.; Monteiro, J.L.; Lobão, M.W.; Santos, T.J. *ESTIMA: A Computer Code for Parameter Estimation and Experiment Design*; Technical Report, PEQ/COPPE/UFRJ: Rio de Janeiro, Brazil, 1993 (in Portuguese).
20. Arnosti Jr., S.; Freire, J.T.; Sartori, D.J.M. Analysis of shrinkage phenomenon in *Brachiaria brizantha* seeds. Drying Technology **2000**, *18* (6), 1339–48.
21. Ciesielczk, W. Analogy of heat and mass transfer during constant rate period in fluidized bed dryer. Drying Technology **1996**, *14* (2), 217–230.